DNA-membrane complex formation during electroporation is DNA size-dependent

Sachdev, Shaurya; Feijoo Moreira, Sara; Keehnen, Yasmine; Rems, Lea; Kreutzer, Michiel T.; Boukany, Pouyan E.

DOI
10.1016/j.bbamem.2019.183089

Publication date
2020

Document Version
Final published version

Published in
Biochimica et Biophysica Acta - Biomembranes

BBA - Biomembranes 1862 (2020) 183089

Contents lists available at ScienceDirect

BBA - Biomembranes

journal homepage: www.elsevier.com/locate/bbamem

DNA-membrane complex formation during electroporation is DNA size-dependent

Shaurya Sachdev, Sara Feijoo Moreira, Yasmine Keehnen, Lea Rems, Michiel T. Kreutzer, Pouyan E. Boukany*

Department of Chemical Engineering, Delft University of Technology, van der Maasweg 9, Delft 2629 HZ, The Netherlands

ARTICLE INFO

Keywords:
Electroporation
Electropermeabilization
Gene electrotransfer
DNA aggregation
DNA-membrane complex formation
DNA size

MSC:
00-01
99-00

ABSTRACT

Size of DNA molecules governs their interaction with the cell membrane during electroporation and their subsequent transport inside the cell. In order to investigate the effect of DNA size on DNA-membrane interaction during electroporation, cells are electro-pulsed with DNA molecules; 15 bp, 25 bp, 50 bp, 100 bp and 1000 bp (bp = base pairs). Within the experimental parameter space, DNA-membrane complexes or DNA aggregates are observed at the cell membrane for DNA molecules containing 25 or more base pairs. No aggregates are observed for DNA molecules containing 15 bp. For all DNA sizes, direct access to the cytoplasm is observed, however the amount translocated decays with the size. The observed dependency of DNA aggregate formation on the size of the DNA molecules is consistent with the Onsager's theory of condensation of anisotropic rod-like molecules.

1. Introduction

The physical and chemical nature of the bio-molecule plays a huge role in electric field mediated molecular delivery [1]. Depending upon the pulse parameters, large nucleic acids such as plasmid DNA (pDNA), enter the cells pre-dominantly via endocytosis after electropermeabilization [2-11]. The endosomal (or endocytotic) cargo is recognized by the cell and handed-off to the intra-cellular pathways after uptake. Their trafficking through the cytoskeleton is mediated by the microtubule network and its associated machinery (dyenin motor) [12-14]. Small nucleic acids, such as small interfering RNA (siRNA), on the contrary enter the cell passively [15-17] and undergo fast, but hindered diffusion through the actin network [18, 19]. The different pathways after uptake have very different outcomes in cargo degradation, chance of reaching their assigned target and, ultimately, therapeutic effect. Electric field mediated DNA delivery has enjoyed success in clinical trials which can be mainly attributed to a trial-and-error based approach of optimization [20, 21]. Further increase in therapeutic efficiency is needed, and can be achieved by understanding the biophysical mechanism of transport [22]. Hence, key to optimization relies on identifying and targeting the rate limiting factors such as mechanisms of cellular uptake and intra-cellular pathways which are highly sensitive to the size of nucleic acids. The influence of size of the nucleic acids on their uptake during electroporation thus plays a crucial role in enhancing the efficiency of electric field mediated gene delivery.

When we focus on the role of nucleic acid size in electroporation (or electropermeabilization), the following experimental and theoretical picture emerges. For lipid vesicles, experiments and theoretical models suggest electrophoresis of DNA molecules through large(-enough) pores formed in the vesicle membrane during electroporation [23, 24]. The influence of size is thus contained in the bulk electrophoretic mobility which in-turn is independent of the size of the DNA molecule [25]. On restricting the pore size to the thickness of a base-pair, the transport is determined by cross-pore electrophoretic mobility and entropic effects from the DNA molecule become dominant. A different theoretical model taking these effects into account suggests that the translocation efficiency follows a power law decay with the size of the DNA molecule [26]. The models and experiments provide the basis for the influence of size of nucleic acids for vesicles where active mechanisms are *de-facto* absent. In case of living cells, plasmid DNA (pDNA) molecules interact with the cell membrane during electric field pulses forming DNA-membrane complexes (referred to as DNA aggregates) at the cell membrane [27, 28]. In a time scale of 10–15 min after pulses, these aggregates are internalized via the active machinery of endocytosis [3-10]. Smaller nucleic acids, such as small interfering RNA (siRNA) [15] and antisene DNA molecules containing Locked Nucleic Acids (LNA/

* Corresponding author.
E-mail address: p.e.boukany@tudelft.nl (P.E. Boukany).

https://doi.org/10.1016/j.bbamem.2019.183089
Received 21 March 2019; Received in revised form 11 September 2019; Accepted 22 October 2019
Available online 31 October 2019

DNA chimeras) [16, 17], have direct access to the cytoplasm during electric field pulses. The influence of size of nucleic acids is manifested distinctly in the form of interaction of these molecules with the cell membrane by forming DNA aggregates. This aggregation of nucleic acids thus provides a signature for identifying the mechanism of nucleic acids uptake and subsequent intra-cellular pathways.

A basis for size dependent aggregation or condensation of DNA molecules can be understood from entropic arguments provided by Onsager's criterion [29]. According to this criterion, rod-like molecules with sufficient anisotropy can condense into a nematic state beyond a critical concentration. In the nematic phase, rod-like molecules gain enough (translational) entropy compared to a randomly oriented isotropic state, sufficient to drive this transition [30]. Such a theory takes into account the size of the molecules, length L and thickness d, predicting the isotropic to nematic transition for $L \geq 4d$ [29]. Nucleic acids of size 25 bp are close to this transition [31].

The experiments and observations are only available for large nucleic acids such as pDNA (4700 bp) and small nucleic acids such as siRNA and LNA/DNA oligomers (20–25 bp). Although the difference in their uptake mechanism during electroporation is widely recognized and acknowledged, there is a huge gap of intermediate sizes for which the uptake mechanism is not identified. This prevents us from obtaining a precise and complete understanding of the influence of the size of nucleic acid on their uptake during electropermeabilization. Very few studies have been performed so far that have systematically investigated the effect of size of the DNA molecules on electroporation mediated nucleic acid delivery. However, they have primarily focussed on either the translocation (cross-membrane transport) [32] or transfection (ultimate gene expression) efficiency as a function of the size of the nucleic acid [32, 33]. Till date no study has focussed on influence of size of the DNA molecule directly on DNA aggregation at the membrane level that could generate much needed insights into the mechanism of uptake and intra-cellular trafficking.

In this paper, we varied the size of the DNA molecules from 15 bp to 1000 bp, in order to investigate its effect on DNA-membrane interaction and cross-membrane transport due to (or during) application of pulsed electric field. This study shows that DNA aggregation at the membrane level is sensitive to the size of the DNA molecules. DNA molecules of size 15 bp had direct access to the cytoplasm and their transport took place without the formation DNA aggregates for the electric pulsing conditions used. DNA molecules of size 25 bp did form DNA aggregates; however, this was a function of electric pulse amplitude. DNA molecules of size 50 bp, 100 bp and 1000 bp showed distinct DNA aggregate formation; however, direct access to the cytoplasm during electric field pulses was also observed for these sizes. This suggests multiple modes of transport for the same size of DNA molecule. Moreover, these results demonstrate that DNA aggregate formation is an onset phenomenon and happens for even small DNA molecules such as 25 bp to 100 bp and is consistent with Onsager's criterion for condensation of rod-like molecules.

2. Materials and methods

2.1. Cell lines and sub-culturing

The Chinese Hamster Ovary cells, CHO-K1 (or CHO), were grown in Nutrient Mixture Ham F-12 (Sigma Aldrich®) supplemented with ≈10% Fetal Bovine Serum (Sigma Aldrich®) and ≈1% Antibiotic-Antimycotic solution (Gibco®). The cells were incubated at 37 °C with 5% CO_2 and the subculture was performed three times a week. For electropulsation experiments, 0.25×10^5 cells were plated (per well) on a μ-slide chambered coverslip of 4 wells (Ibidi®), with 500 μl of culture medium 24 h before the application of the electric pulses.

Human lung carcinoma cells, A549, were grown in a medium consisting of Dulbecco's Modified Eagle's Medium (Sigma Aldrich®) supplemented with ≈10% Fetal Bovine Serum (FBS) (Sigma Aldrich®) and ≈1% Antibiotic-Antimycotic solution (Gibco®). The cells were incubated at 37 °C with 5% CO_2 and the subculture was performed three times a week. For electropulsation of A549 cells, 0.30×10^5 cells were plated (per well) on a μ-slide chambered coverslip of 4 wells (Ibidi®) with 500 μl of culture medium 24 h before the application of the electric pulses.

2.2. DNA fragments and staining

DNA fragments of different sizes (1000 bp, 100 bp, 50 bp, 25 bp and 15 bp) were purchased from ThermoFisher® under the brand of NoLimits™ DNA. Each DNA fragment stock vial consisted of 10 μg of DNA at a concentration of 0.5 μg/μl in 10 mM Tris–HCl(pH 7.6) and 1 mM EDTA. The DNA molecules were stained in the stock vials using YOYO-1 dye (1 mM in DMSO from ThermoFisher®). This dye has been commonly used to visualize DNA molecules under physical forces [34]. The bp:YOYO-1 dye molecule staining ratio was kept constant at 10:1 for all the experiments and staining was performed on ice for 1 hour. Such a staining ratio is known to cause a 15% reduction in electrophoretic mobility of DNA molecule which is predominantly attributed to a reduction in the net effective charge of the YOYO-1-DNA complex [35, 36].

2.3. Electropulsation of cells

Just before the electropulsation experiments, the cells were taken out of the incubator and the culture medium was removed from the μ-slide and the cells were washed twice with Dulbecco's Phosphate Buffered Saline from Sigma Aldrich®. The chambers were then filled with 500 μl of pulsing buffer (10 mM KH_2PO_4/Na_2HPO_4, 1 mM $MgCl_2$ and 250 mM sucrose at a pH of 7.4) containing 10 μg/ml of stained DNA solution. Stainless steel electrodes of 3 mm gap were immersed in the chamber and fixed to the walls to ensure a uniform electric field distribution. To apply the electric field, these electrodes were connected to a cell electropulsator (BetaTech Electro cell B10 HV-LV, France), which can deliver unipolar and bipolar square-wave pulses. All experiments were conducted at room temperature and atmospheric pressure. The maximum time allowed for the cells to be out of the incubator during all the experiments was 30 min.

2.4. Confocal imaging of DNA uptake

To image the localization and dynamics of DNA molecules, experiments were performed on a confocal microscope (ZEISS LSM 710, Germany). 488 nm Argon laser was used to excite the YOYO-1 labelled DNA molecules and the images were acquired using a 40× (1.3 NA oil immersion) objective. The scanning speed of the laser was adjusted to obtain a pixel dwell of 7.04 μs. The field of view consisted of 1836×1836 pixels spanning $212.55 \times 212.55\ \mu m^2$. All the images were acquired at an 8-bit pixel depth.

3. Results

In order to observe the effect of DNA size on electric field mediated DNA delivery, linear DNA fragments of size 15 bp, 25 bp, 50 bp, 100 bp and 1000 bp were chosen. All DNA fragments were fluorescently labelled with YOYO-1 dye. The effect of DNA size was then observed in terms of fluorescence intensity of DNA molecules interacting with the cell membrane (as DNA aggregates) after the application of electric pulses. The results are shown in Fig. 1.

Fig. 1 (a) shows CHO cells before application of electric pulses for all DNA sizes. Fluorescently labelled DNA molecules were found to be homogeneously distributed around the cells and no DNA membrane interaction or penetration of DNA molecules into the cells was observed. After applying a train of 10 electric field pulses at an amplitude of 0.4 kV/cm with a pulse duration of 5 ms and at a frequency of 1 Hz,

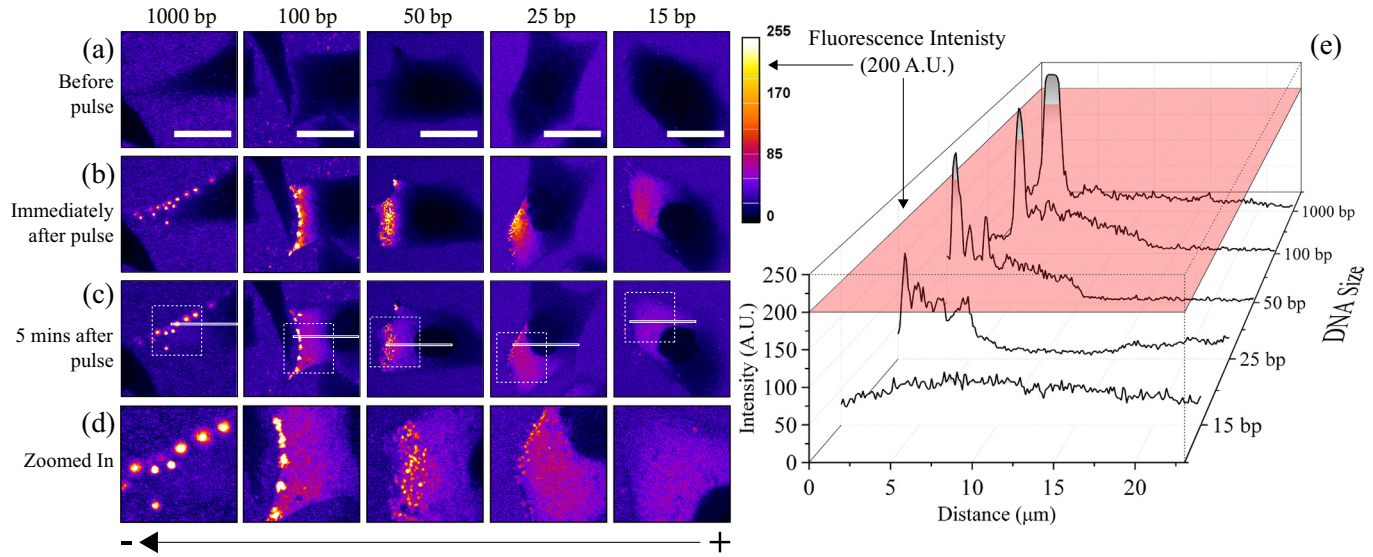

Fig. 1. Figure showing representative CHO cells before and after the application of electric pulses. The images are color coded according to the intensity of fluorescently labelled DNA molecules. The color bar represents the corresponding fluorescence intensity values. (a) Represents the state of the cell before the application of electric pulses. Scale bar = 20 μm. (b) Represents the state of the cell immediately (within ≈1 min) after the application of electric pulses. The electric pulse amplitude was 0.4 kV/cm with a pulse duration of 5 ms. 10 pulses were applied at a frequency of 1 Hz. (c) Represents the state of the cell 5 min after the application of electric pulses. (d) Shows a zoomed-in view of the cells 5 min after the electric pulses were applied. The field of view in (d) is defined by the dotted white box drawn in (c). In each experiment the size of the DNA molecules was varied as indicated above each column. The direction of applied electric field is indicated by the arrow shown below (d). (e) Shows the fluorescence intensity profiles along the solid white box drawn in (c).

DNA molecules were found to both interact with the membrane, and also be delivered into the cells. This is shown in Fig. 1 (b) (Immediately after pulse) for each size of DNA studied. DNA membrane interaction or DNA aggregation at the membrane was observed for 1000 bp, 100 bp, 50 bp and 25 bp as local bright spots of high fluorescence intensity. Direct access of DNA molecules to the cytoplasm was observed for all DNA sizes as seen by a homogeneous fluorescence intensity inside the cells. The cells were allowed to rest, and observations were made again after 5 min of applying the electric pulses. This was done in order to distinguish the locally accumulated but free DNA from aggregated DNA at the membrane, as the primary contributor towards local bright spots. From Fig. 1 (c) (5 min after pulse), it can be seen that the bright spots remain similar in number and area (to the corresponding images in Fig. 1 (b)) for DNA sizes of 1000 bp, 100 bp and 50 bp. However, a lot of bright spots that were seen for 25 bp (Fig. 1 (b)) were no longer present 5 min after pulse (Fig. 1 (c)), rendering them as mainly accumulated but free DNA rather than aggregated DNA. Fig. 1 (d) shows zoomed in view of cells 5 min after the application of electric pulses for the dotted white boundaries depicted in Fig. 1 (c), to clearly indicate the DNA aggregates as local bright spots, as observed for DNA size of 1000 bp, 100 bp and 50 bp. Experiments using bipolar electric pulses were also done to confirm that these bright spots are stable DNA aggregates for both CHO and A549 cells (see Supplementary information — Section 1).

Fig. 1 (e) shows fluorescence intensity profiles along the region marked by solid white box in Fig. 1 (c) for each DNA size. The profiles correspond to the fluorescence intensity along the penetration distance into the cell and are averaged along the width of the box. It can be seen that the fluorescence intensity peaks near the cell membrane for the DNA sizes that form aggregates (1000 bp, 100 bp, 50 bp). The peaks in the profile correspond to fluorescence from DNA aggregates that are located on the edge of the cell membrane. On penetrating further into the cell the fluorescence intensity drops but is still greater than zero. This fluorescence was not present before the application of electric pulses and hence correspond to free DNA that has been translocated into the cell in non-aggregated form.

The fluorescence intensity profiles in Fig. 1 (e) suggest that aggregated DNA can be distinguished from free DNA by choosing an appropriate fluorescence intensity threshold. Since the peaks along the profile reach a minimum value of 200 A.U. (Arbitrary Units) when DNA aggregates are formed, as can be seen by the pink cutting-plane in Fig. 1 (e), it can be argued that DNA aggregates have at least a fluorescence intensity of 200 A.U. On the contrary the free DNA inside the cytoplasm correspond to a fluorescence intensity < 200 A.U. Therefore, we chose the fluorescence intensity of 200 A.U. as the threshold to distinguish between aggregated DNA at the membrane and free DNA inside the cytoplasm.

The distinction between fluorescence intensity of aggregated DNA and free DNA, based on a threshold described in Fig. 1 (e), is used to analyse their cellular uptake separately and independently, as a function of DNA size. Fig. 2 (a) shows a representative CHO cell (5 min after the application of electric pulses) for a DNA size of 50 bp. Segmenting the image with a threshold intensity of 200 A.U. divides the image into two parts: a region with aggregated DNA (> 200 A.U.) and region with free DNA (< 200 A.U.). The boundaries dividing these two regions are shown in Fig. 2 (b) marked in red. The regions depicting aggregated DNA are shown in Fig. 2 (c), filled in green. In order to get more insights into the effect of DNA size on aggregation of DNA molecules, the apparent area of these regions (fluorescence intensity > 200 A.U.) was calculated for a number of cells, 5 min after the application of electric pulses, for each DNA size. The resulting net aggregated area was summed up for each DNA size and normalized by the number of cells analysed. This is shown in Fig. 2 (e) and (f) for CHO and A549 cells respectively, and for two different electric pulse amplitudes. Experiments were done on two different cell lines (CHO and A549) to check the consistency of the trend. To further confirm the trend observed, a second independent set of experiments was performed for DNA size of 25–100 bp, and the data is shown in Section 4 of Supplementary information. Since 15 bp DNA did not show any aggregate formation, the aggregated area per cell is almost 0. The aggregated area per cell for DNA molecules of size 25 bp is only slightly higher than for 15 bp and is consistent with the observations in Fig. 1 (c–e) for 25 bp. On increasing the size of DNA further, the apparent area per cell of aggregated DNA molecules increases further for both the cell lines (CHO and A549). It should also be noted that a higher electric field intensity led to an

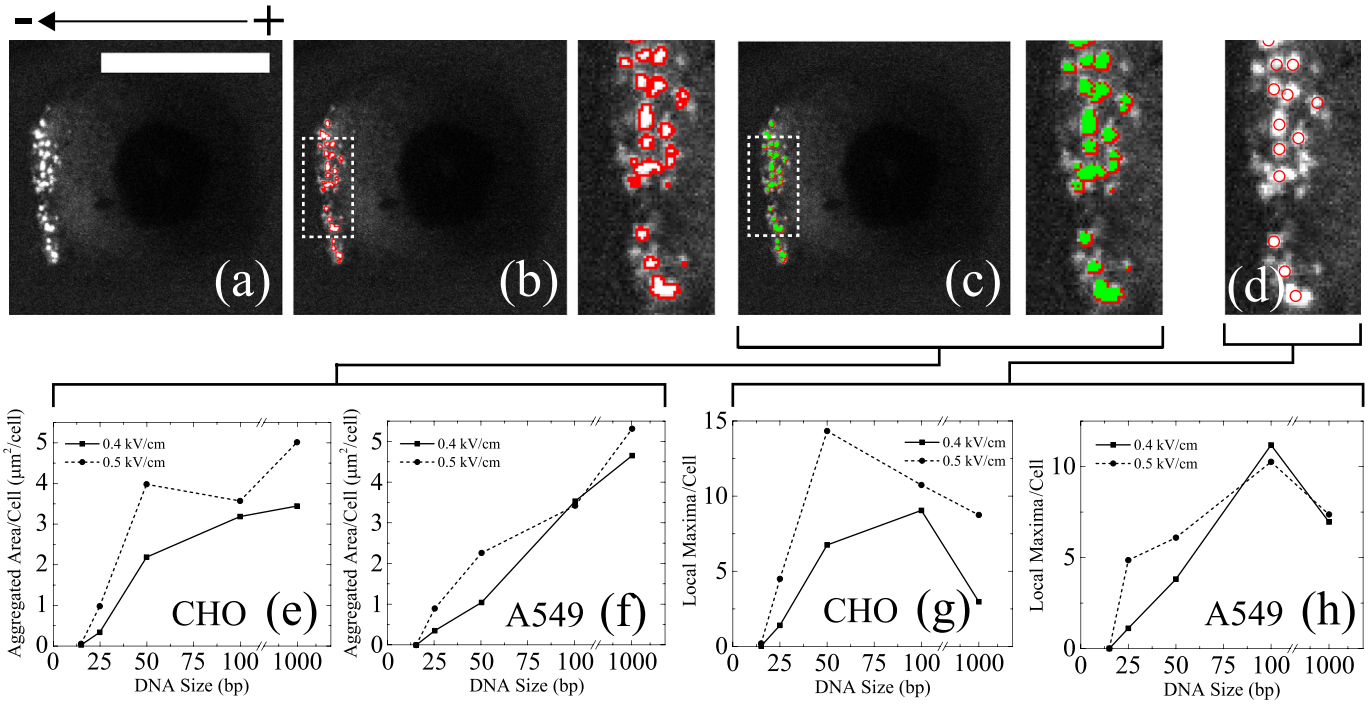

Fig. 2. Characterization of DNA aggregates. (a) Image of a representative CHO cells 5 min after the application of electric pulses with DNA molecules of size 50 bp. Scale bar = 20 μm. The electric pulse amplitude was 0.4 kV/cm with a pulse duration of 5 ms. 10 pulses were applied at a frequency of 1 Hz. (b) The image in (a) was segmented applying a fluorescence intensity threshold of 200 A.U. resulting in two regions of high (> 200 A.U.) and low (< 200 A.U.) fluorescence intensities demarcated by a red outline. (c) High fluorescence intensity region (> 200 A.U.) is depicted coloured in green. (d) Local maxima or DNA aggregates detected by applying Gaussian filters (see Supplementary information — Section 2 for detailed algorithm of local maxima detection). Aggregated area per cell as a function of size of the DNA molecule for (e) CHO and (f) A549 cell lines. Number of local maxima detected as a function of size of the DNA molecule for (g) CHO and (h) A549 cell lines. For each data point in (e)–(h), 45 cells on average were analysed with a minimum of 25 cells and maximum of 81 cells.

increase in the aggregated DNA area per cell. This is especially pronounced for a DNA size of 25 bp, where a considerably higher amount of DNA molecules was found to interact with the membrane forming DNA aggregates.

Apart from aggregated area per cell, the number of aggregates per cell was calculated by applying Gaussian filters to the images and identifying the DNA aggregates (or bright spots) as local maxima. These local maxima of fluorescence intensity are identified in red circles in Fig. 2 (d) on DNA aggregates for the same representative CHO cell as in Fig. 2 (a) –(c). The detailed algorithm for detecting the number of DNA aggregates as local maxima is given in Supplementary information — Section 2. The total number of local maxima was calculated for a number of cells, for each DNA size, and then normalized by the number of cells analysed. The same cells were analysed to calculate local maxima as in Fig. 2 (e) and (f). Fig. 2 (g) and (h) shows the number of local maxima per cell as a function of DNA size for CHO and A549 cells, respectively, and for two different electric pulse amplitudes. The number of local maxima per cell follows a similar behaviour as the net aggregated DNA area/cell shown in Fig. 2 (f). However, there is a dip in the number of aggregates for a 1000 bp. This dip could possibly be explained by the fact that the experiments were done by keeping the DNA concentration constant at 10 μg/ml. Thus, the cells were always exposed to the same number of base-pairs but the number of DNA molecules was decreasing with increasing DNA size.

Increasing DNA size increases the contribution towards aggregated DNA as seen by the aggregated DNA area per cell and number of local maxima per cell in Fig. 2 (e–h). By segmenting the image and considering fluorescence intensity < 200 A.U., a similar analysis can be done for free DNA. This is shown in Fig. 3. A representative CHO cell is shown in Fig. 3 (a) 5 min after the application of electric pulses for a DNA size of 50 bp. The image is segmented with a threshold fluorescence intensity of 200 A.U. and the segmentation result is demarcated by red outlines. The cell contour is shown in cyan. The algorithm for determining the cell contour is shown in Supplementary information — Section 3. The region corresponding to a fluorescence intensity < 200 A.U., filled in green is shown in Fig. 3 (b). The mean fluorescence intensity within this region is calculated for each individual cell after 5 min of electric pulse application (I_{after}). The mean fluorescence intensity before the application of electric pulses (I_{before}), within the same region (shown in green), is subtracted from this value in order to estimate the fluorescence intensity of free DNA translocated inside the cytoplasm as $I = I_{after} - I_{before}$. After normalizing with the mean fluorescence intensity of DNA molecules outside the cells (I_o), the corresponding result (I/I_o) is plotted in Fig. 3 (c) and (d) as a function of DNA size and for CHO and A549 cell lines, respectively, and for two different electric pulse amplitudes. Contrary to aggregated DNA, the fluorescence intensity of free DNA decreases with increasing DNA size.

4. Discussion

Our results indicate that DNA aggregation at the cell membrane is not only observed for large DNA sizes such as 1000 bp, as previously reported in literature, but also for small DNA sizes of 25 bp, 50 bp and 100 bp. With an increasing size there is an increasing tendency for the DNA molecules to aggregate at the cell membrane. At the same time, the amount of DNA that has direct access to the cytoplasm (free DNA) tends to decreases with the size of the DNA molecule. Such a dependency of amount of aggregated and free DNA on the size of the DNA molecule is discussed below with possible suggestions for the mechanism of DNA aggregation.

Aggregated DNA can be considered to be in a different physical state compared to bulk DNA. Due to localized high fluorescence intensity of DNA aggregates, this state can be referred to as a condensed state of DNA molecules. Persistence length of DNA under physiological

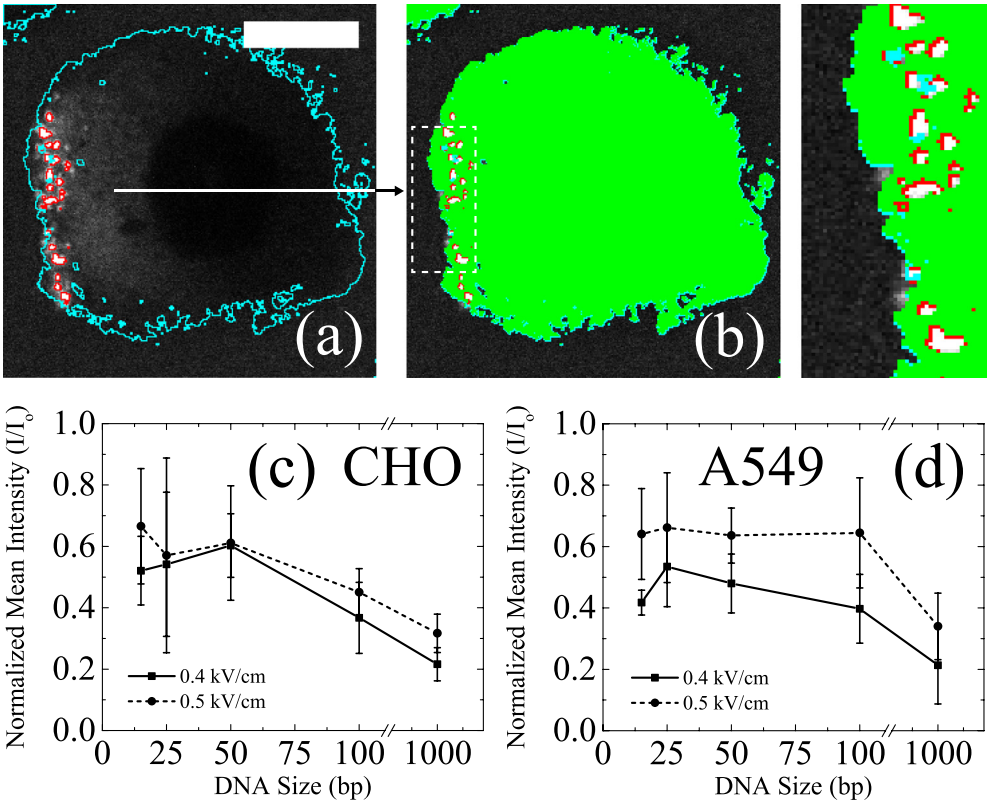

Fig. 3. Characterization of free DNA that has direct access to the cytoplasm. (a) Image of a representative CHO cells 5 min after the application of electric pulses with DNA molecules of size 50 bp. Scale bar = 10 μm. The electric pulse amplitude was 0.4 kV/cm with a pulse duration of 5 ms. 10 pulses were applied at a frequency of 1 Hz. The image was segmented by applying a fluorescence intensity threshold of 200 A.U. resulting in two regions of high (> 200 A.U.) and low (< 200 A.U.) fluorescence intensities demarcated by a red outline. The cell contour is demarcated by a cyan outline. (b) Low fluorescence intensity region (< 200 A.U.) is coloured in green. (c) Mean fluorescence intensity of free DNA (green region) as a function of the size of DNA molecule is shown in (c) and (d) for CHO and A549 cell lines, respectively. The error bar represents standard deviation around the average of the mean fluorescence intensity of free DNA depicted by the region coloured in green in each cell. For each data point in (c) and (d), 11 cells were analysed on average with a minimum of 5 cells and a maximum of 22 cells.

conditions is around 50 nm or 150 bp [37, 38]. Therefore, DNA molecules of size 15 bp, 25 bp, 50 bp and 100 bp are essentially rod-like molecules, whereas DNA molecules of size 1000 bp are coiled. Condensation of rod-like molecules, by increasing the concentration, was first described by Onsager in 1949 [29]. According to his theory, rod-like molecules can condense into liquid crystal (nematic) phases, if they posses sufficient anisotropy; L ≥ 4d, where L is the length of the molecule and d is the thickness (or diameter) of the molecule. If we consider the thickness of DNA molecules to be around 2 nm and the inter-base-pair distance to be 0.34 nm [39], DNA molecules of size ~25 bp and higher possess sufficient anisotropy as required by the Onsager's criterion to be condensed into a nematic phase. On the other hand, DNA molecules of size 15 bp are sufficiently isotropic and hence will not condense into a nematic phase. We observed aggregates for DNA molecules of size 25 bp and higher, and no aggregates were observed for a DNA size of 15 bp consistent with Onsager's criterion.

Isotropic to nematic phase transition of hard rods was proposed for a 3-dimensional system [29]. In case of electroporation, it is believed that DNA molecules are adsorbed on the cell membrane by the divalent cations, which enhance DNA aggregation [3]. Moreover, even after applying bipolar pulses, the aggregates remained anchored to the membrane (see Supplementary information — Section 1). During electroporation, we are primarily dealing with a 2-dimensional system. Onsager's criteria for the isotropic-nematic phase transition (L ≥ 4d) was also shown to be valid for a 2-dimensional system of adsorbed short DNA strands confined between lipid bilayers [40]. In another study, it was shown that DNA origami nano-needles with sufficient anisotropy adsorbed on a lipid bilayer of a GUV, underwent an isotropic to nematic phase transition beyond a critical surface charge density [41]. These DNA nano-needles formed locally ordered domains in the nematic phase that were below 1 μm in size, consistent with the size of DNA aggregates that we observed (around 200–500 nm).

Based on entropic arguments by Onsager, an extremely high concentration is required to condense DNA into a nematic phase [29, 31]. It is possible that such high concentrations are never achieved by a non-permeabilizing electric field. However, upon permeabilization, electric field lines concentrate and penetrate the permeable sites on the cell membrane [42, 43]. Due to local enhancement of electric field at these permeable sites, the DNA molecules should also get concentrated, possibly reaching high enough concentrations required for the isotropic to nematic phase transition to kick in. Experiments were done for 2 different values of electric field intensities above the permeabilizing threshold. A general trend observed was that with higher electric field intensity, more DNA aggregates were observed. With an increasing field intensity, the permeabilized area is increased [44, 45], which could in principle account for higher number DNA aggregates per cell.

In addition, such a phenomenon also explains why DNA molecules are not only found in the aggregated state, but also have direct access to the cytoplasm. With a permeable electric field, the adsorbed DNA molecules can get locally accumulated at the permeable sites. As the size of the DNA molecules increases, its tendency, owing to its increasing anisotropy, to condense or aggregate increases (Fig. 2). At the same time its tendency to translocate through the permeable structures and gain direct access to the cytoplasm decreases (Fig. 3). During electroporation, it is also believed that there is a heterogenous population of the size of these permeable sites or defects [46, 47], with longer pulses tending to favour a population of larger pores [48, 49]. It is possible that DNA molecules that gain direct access to the cytoplasm, enter the cells primarily through these permeable sites [2, 50, 51]. With a larger pore size there is an increasing probability that DNA molecules can translocate without getting stuck at the membrane. These observations are consistent with 2 classes of DNA molecules we observed, DNA molecules in the aggregated state at the membrane, and DNA molecules that have direct access to the cytoplasm.

For DNA molecules that have direct access to the cytoskeleton, relative contributions of electrophoretic drift and diffusion can be understood using the Péclet number (*Pe*). The Péclet number is defined by $Pe = t_{diffusion}/t_{drift}$, which compares the time-scale of diffusion $t_{diffusion}$, to the time-scale of drift t_{drift} [52]. The diffusive time scale can be defined by $t_{diffusion} = L^2/D$, where L is an appropriate length scale and D is

the diffusion coefficient. The drift time can be defined by $t_{drift} = L/v$. Thus, the Péclet number is defined as $Pe = vL/D$. For transport of DNA molecules through bulk, $v = \mu E$, where μ is the electrophoretic mobility of the DNA molecule and E is the applied electric field. Therefore, the bulk Péclet number is $Pe = (\mu E R_o)/D$, where radius of cells R_o is considered as an appropriate length scale. For permeabilizing electric field, $ER_o \sim 1$ V, according to Schwan equation [53], and as also considered in Ref. [23]. Therefore, the Péclet number for bulk transport of DNA molecules is $Pe \sim \mu/D(1\text{ V})$. The electrophoretic mobility of DNA molecules of size 15 bp–100 bp, can be considered as $\mu \sim 3.2 \times 10^{-4}\,cm^2\,V^{-1}\,s^{-1}$ [54, 55], and the diffusion coefficient can be considered as $D \sim 6.5 \times 10^{-6}\,cm^2\,s^{-1}\,bp^{-0.68}$ [18]. With these values the Péclet number is $Pe \sim 50\,(bp)^{0.68}$. Thus, for DNA sizes between 15 bp and 100 bp, Pe varies between 300 and 1200, implying that electrophoretic drift dominates diffusion for transport of DNA molecules in bulk during the electric field pulse. These estimates also support the hypothesis that DNA becomes highly concentrated next to the membrane during the pulse.

For transport through the pore, the Péclet number can be considered as $Pe_{pore} = \nu_{pore} L/D_{pore}$, where ν_{pore} is the velocity and D_{pore} is the diffusivity, of the translocating DNA molecule through the pore. Contour length of the DNA molecule (L_c) can be considered as an appropriate length scale (L). Precise determination of ν_{pore} and D_{pore} is beyond the scope of this work, however some estimates can be provided considering the framework followed in Ref. [54]. As shown in Ref. [54], ν_{pore}/D_{pore} was independent of the applied potential difference, for a DNA size of 500 bp. $\nu_{pore}/D_{pore} = 0.15 \pm 0.1\ nm^{-1}$, for DNA translocating through pores of diameter 2.6 –6 nm, similar to electro-pore diameters. Thus, Péclet number can be considered as $Pe_{pore} \sim 0.15 L_c$. For DNA sizes of 15–100 bp $L_c = 0.34 \times$ bp nm and hence Pe_{pore} ranges between ~0.7 and 5. This indicates similar contributions of electrophoretic drift and diffusion for DNA molecules translocating through a pore. It should be noted that the applied potential difference (~0.20 –0.35 V) and the aqueous solution across each side of the pore was different in Ref. [54]. In our experiments, DNA molecules encounter the cytoskeleton while translocating through the electro-pore. In this case, the diffusion coefficient is lower [19], and might make electrophoretic drift as the dominant mode of transport of DNA molecules through the membrane.

Onsager's theory seems to describe the dependency of the size of the DNA molecule on DNA aggregate formation at the cell membrane during electroporation. However, it must be noted that high concentrations (≈500 mg/ml) are required for the isotropic to nematic phase transition (based on entropic arguments) [29, 31]. There are also other mechanisms which can lead to DNA condensation and do not require such high concentrations. A common method to condense and precipitate DNA molecules is to use multivalent cations [56, 57]. For instance multivalent poly-amine cations (tri-valent and tetra-valent) caused condensation of 25 bp DNA molecules [58]. In this case, counter-ion induced attraction of the DNA molecules was most likely the reason for DNA condensation, and the condensed DNA molecules could be found in liquid crystal phases. Divalent cations have also been shown to condense DNA molecules in 2-dimensions [59]. DNA molecules adsorbed on a GUV through cationic lipids collapsed into a condensed phase through curvature mediated interactions [60, 61]. Thus, the origin of condensation or aggregation of DNA molecules is different in these cases (divalent cations or curvature mediated) compared to Onsager's criterion (high concentration), however their dependency on the size of the DNA molecule, to the best of our knowledge, is not explored. Thus, there is a possibility that the DNA molecules are condensing and aggregating at the cell membrane through different pathways during electroporation and further research is necessary to completely elucidate the origins and the nature of these DNA aggregates.

5. Conclusion

DNA aggregate formation was not only observed for large DNA molecules of size of 1000 bp but also for short DNA molecules of size 25 bp, 50 bp and 100 bp, whose persistence length is larger than the contour length, and hence behave as rod-like molecules. No DNA aggregates were observed for a DNA size of 15 bp. With increasing DNA size the tendency of the DNA molecules to aggregate increased, while the tendency to translocate freely into the cytoplasm decreased. In doing so, we probed the effects of size and anisotropy of the DNA molecules on the DNA-membrane complex formation. These observations are consistent with the Onsager's theory of condensation of rod-like molecules.

Transparency document

The Transparency document associated with this article can be found, in online version.

Acknowledgments

We acknowledge financial support from European Research Council (ERC) under the European Union's Seventh Framework Programme (FP/2007-2013)/ERC Grant, Agreement No. 337820. S.F.M acknowledges the support from Fundación Barrié (Spain).

Appendix A. Supplementary data

Supplementary data to this article can be found online at https://doi.org/10.1016/j.bbamem.2019.183089.

References

[1] M.P. Stewart, R. Langer, K.F. Jensen, Intracellular delivery by membrane disruption: mechanisms, strategies, and concepts, Chem. Rev. 118 (16) (2018) 7409–7531.
[2] C. Rosazza, S. Haberl Meglic, A. Zumbusch, M.-P. Rols, D. Miklavcic, Gene electrotransfer: a mechanistic perspective, Curr. Gene Ther. 16 (2) (2016) 98–129.
[3] M. Wu, F. Yuan, Membrane binding of plasmid DNA and endocytic pathways are involved in electrotransfection of mammalian cells, PloS one 6 (6) (2011) e20923.
[4] C. Rosazza, E. Phez, J.-M. Escoffre, L. Cézanne, A. Zumbusch, M.-P. Rols, Cholesterol implications in plasmid DNA electrotransfer: evidence for the involvement of endocytotic pathways, Int. J. Pharm. 423 (1) (2012) 134–143.
[5] C. Rosazza, H. Deschout, A. Buntz, K. Braeckmans, M.-P. Rols, A. Zumbusch, Endocytosis and endosomal trafficking of DNA after gene electrotransfer in vitro, Mol Ther. Nucleic Acids 5 (2016).
[6] B. Markelc, E. Skvarca, T. Dolinsek, V.P. Kloboves, A. Coer, G. Sersa, M. Cemazar, Inhibitor of endocytosis impairs gene electrotransfer to mouse muscle in vivo, Bioelectrochemistry 103 (2015) 111–119.
[7] C.-C. Chang, M. Wu, F. Yuan, Role of specific endocytic pathways in electrotransfection of cells, Mol. Therapy-Methods & Clin. Dev. 1 (2014).
[8] L.D. Cervia, C.-C. Chang, L. Wang, F. Yuan, Distinct effects of endosomal escape and inhibition of endosomal trafficking on gene delivery via electrotransfection, PloS one 12 (2) (2017) e0171699.
[9] M. Mao, L. Wang, C.C. Chang, K.E. Rothenberg, J. Huang, Y. Wang, B.D. Hoffman, P.B. Liton, F. Yuan, Involvement of a Rac1-dependent macropinocytosis pathway in plasmid DNA delivery by electrotransfection, Mol. Ther. 25 (3) (2017) 803–815.
[10] L. Wang, S.E. Miller, F. Yuan, Ultrastructural analysis of vesicular transport in electrotransfection, Microsc. Microanal. 24 (5) (2018) 553–563.
[11] M. Pavlin, M. Kandušer, New insights into the mechanisms of gene electrotransfer—experimental and theoretical analysis, Sci. rep. 5 (2015) 9132.
[12] E.E. Vaughan, D.A. Dean, Intracellular trafficking of plasmids during transfection is mediated by microtubules, Mol. Ther. 13 (2) (2006) 422–428.
[13] E.E. Vaughan, R.C. Geiger, A.M. Miller, P.L. Loh-Marley, T. Suzuki, N. Miyata, D.A. Dean, Microtubule acetylation through HDAC6 inhibition results in increased transfection efficiency, Mol. Ther. 16 (11) (2008) 1841–1847.
[14] C. Rosazza, A. Buntz, T. Rieß, D. Wöll, A. Zumbusch, M.-P. Rols, Intracellular tracking of single-plasmid DNA particles after delivery by electroporation, Mol. Ther. 21 (12) (2013) 2217–2226.
[15] a. Paganin-Gioanni, E. Bellard, J.M. Escoffre, M.P. Rols, J. Teissié, M. Golzio, Direct visualization at the single-cell level of siRNA electrotransfer into cancer cells, Proc. Natl. Acad. Sci. U. S. A. 108 (26) (2011) 10443–10447.
[16] S. Chabot, J. Orio, R. Castanier, E. Bellard, S.J. Nielsen, M. Golzio, J. Teissié, LNA-

based oligonucleotide electrotransfer for miRNA inhibition, Mol. Ther. 20 (8) (2012) 1590–1598.
[17] S. Chabot, J. Teissié, M. Golzio, Targeted electro-delivery of oligonucleotides for RNA interference: siRNA and antimiR, Adv. Drug Delivery Rev. 81 (2015) 161–168.
[18] G.L. Lukacs, P. Haggie, O. Seksek, D. Lechardeur, N. Freedman, A. Verkman, Size-dependent DNA mobility in cytoplasm and nucleus, J. Biol. Chem. 275 (3) (2000) 1625–1629.
[19] E. Dauty, A. Verkman, Actin cytoskeleton as the principal determinant of size-dependent DNA mobility in cytoplasm a new barrier for non-viral gene delivery, J. Biol. Chem. 280 (9) (2005) 7823–7828.
[20] L. Lambricht, A. Lopes, S. Kos, G. Sersa, V. Préat, G. Vandermeulen, Clinical potential of electroporation for gene therapy and DNA vaccine delivery, Expert Opin. Drug Delivery 13 (2) (2016) 295–310.
[21] R. Heller, L.C. Heller, Gene electrotransfer clinical trials, Advances in Genetics, 89 Elsevier, 2015, pp. 235–262.
[22] L.D. Cervia, F. Yuan, Current progress in electrotransfection as a nonviral method for gene delivery, Mol. Pharm. 15 (9) (2018) 3617–3624.
[23] T. Portet, C. Favard, J. Teissié, D.S. Dean, M.-P. Rols, Insights into the mechanisms of electromediated gene delivery and application to the loading of giant vesicles with negatively charged macromolecules, Soft Matter 7 (8) (2011) 3872–3881.
[24] D.L. Perrier, L. Rems, P.E. Boukany, Lipid vesicles in pulsed electric fields: fundamental principles of the membrane response and its biomedical applications, Adv. Colloid Interface Sci. 249 (2017) 248–271.
[25] N.C. Stellwagen, C. Gelfi, P.G. Righetti, The free solution mobility of DNA, Biopolymers: Orig. Res. Biomolecules 42 (6) (1997) 687–703.
[26] M. Yu, W. Tan, H. Lin, A stochastic model for DNA translocation through an electropore, Biochim. Biophys. Acta. (BBA)-Biomembranes 1818 (11) (2012) 2494–2501.
[27] M. Golzio, J. Teissie, M.-P. Rols, Direct visualization at the single-cell level of electrically mediated gene delivery. Proc. Natl. Acad. Sci. U. S. A. 99 (3) (2002) 1292–1297.
[28] E. Neumann, Membrane electroporation and direct gene transfer, Bioelectrochem. Bioenerget. 28 (1-2) (1992) 247–267.
[29] L. Onsager, The effects of shape on the interaction of colloidal particles, Ann. N. Y. Acad. Sci. 51 (4) (1949) 627–659.
[30] D. Frenkel, Perspective on The effect of shape on the interaction of colloidal particles, Theoretical Chemistry Accounts, Springer, 2000, pp. 212–213.
[31] M. Nakata, G. Zanchetta, B.D. Chapman, C.D. Jones, J.O. Cross, R. Pindak, T. Bellini, N.A. Clark, End-to-end stacking and liquid crystal condensation of 6-to 20-base pair DNA duplexes, Science 318 (5854) (2007) 1276–1279.
[32] B.D. Hornstein, D. Roman, L.M. Arévalo-Soliz, M.A. Engevik, L. Zechiedrich, Effects of circular DNA length on transfection efficiency by electroporation into HeLa cells, PloS one 11 (12) (2016) e0167537.
[33] T. Xie, T.Y. Tsong, Study of mechanisms of electric field-induced DNA transfection. III. Electric parameters and other conditions for effective transfection, Biophys. J. 63 (1) (1992) 28–34.
[34] L. Rems, D. Kawale, L.J. Lee, P.E. Boukany, Flow of DNA in micro/nanofluidics: from fundamentals to applications, Biomicrofluidics 10 (4) (2016) 043403.
[35] C. Carlsson, A. Larsson, M. Jonsson, Influence of optical probing with YOYO on the electrophoretic behavior of the DNA molecule, Electrophoresis 17 (4) (1996) 642–651.
[36] H.R. Reese, Effects of DNA charge and length on the electrophoretic mobility of intercalated DNA, Biopolymers: Orig. Res. Biomol. 34 (10) (1994) 1349–1358.
[37] S. Pan, D. At Nguyen, T. Sridhar, P. Sunthar, J. Ravi Prakash, Universal solvent quality crossover of the zero shear rate viscosity of semidilute DNA solutions, J. Rheol. 58 (2) (2014) 339–368.
[38] A. Brunet, C. Tardin, L. Salome, P. Rousseau, N. Destainville, M. Manghi, Dependence of DNA persistence length on ionic strength of solutions with monovalent and divalent salts: a joint theory-experiment study, Macromolecules 48 (11) (2015) 3641–3652.
[39] M. Mandelkern, J.G. Elias, D. Eden, D.M. Crothers, The dimensions of DNA in solution, J. Mol. Evol. 152 (1) (1981) 153–161.
[40] N.F. Bouxsein, C. Leal, C.S. McAllister, K.K. Ewert, Y. Li, C.E. Samuel, C.R. Safinya, Two-dimensional packing of short DNA with nonpairing overhangs in cationic liposome-DNA complexes: from onsager nematics to columnar nematics with finite-length columns, J. Am. Chem. Soc. 133 (19) (2011) 7585–7595.
[41] A. Czogalla, D.J. Kauert, R. Seidel, P. Schwille, E.P. Petrov, DNA origami nanoneedles on freestanding lipid membranes as a tool to observe isotropic-nematic transition in two dimensions, Nano Lett. 15 (1) (2014) 649–655.
[42] J.C. Neu, K.C. Smith, W. Krassowska, Electrical energy required to form large conducting pores, Bioelectrochemistry 60 (1-2) (2003) 107–114.
[43] J. Li, H. Lin, The current-voltage relation for electropores with conductivity gradients, Biomicrofluidics 4 (1) (2010) 013206.
[44] B. Gabriel, J. Teissié, Direct observation in the millisecond time range of fluorescent molecule asymmetrical interaction with the electropermeabilized cell membrane, Biophys. J. 73 (5) (1997) 2630–2637.
[45] J.-M. Escoffre, E. Bellard, E. Phez, M.-P. Rols, C. Favard, Effect of electric field intensity on plasmid DNA/membrane interaction during in-vitro gene electrotransfer, Drug Delivery Lett. 2 (1) (2012) 22–25.
[46] D. Chang, T.S. Reese, Changes in membrane structure induced by electroporation as revealed by rapid-freezing electron microscopy, Biophys. J. 58 (1) (1990) 1–12.
[47] J.T. Sengel, M.I. Wallace, Imaging the dynamics of individual electropores, Proc. Natl. Acad. Sci. 113 (19) (2016) 5281–5286.
[48] J. Teissie, M. Golzio, M. Rols, Mechanisms of cell membrane electropermeabilization: a minireview of our present (lack of?) knowledge, Biochim. Biophys. Acta. (BBA)-General Subjects 1724 (3) (2005) 270–280.
[49] R.S. Son, K.C. Smith, T.R. Gowrishankar, P.T. Vernier, J.C. Weaver, Basic features of a cell electroporation model: illustrative behavior for two very different pulses, J. Membr. Biol. 247 (12) (2014) 1209–1228.
[50] J.-M. Escoffre, T. Portet, C. Favard, J. Teissié, D.S. Dean, M.-P. Rols, Electromediated formation of DNA complexes with cell membranes and its consequences for gene delivery, Biochim. Biophys. Acta (BBA)-Biomembranes 1808 (6) (2011) 1538–1543.
[51] J. Teissie, Electrically mediated gene delivery: basic and translational concepts, Novel Gene Therapy Approaches, IntechOpen, 2013.
[52] T.M. Squires, S.R. Quake, Microfluidics: fluid physics at the nanoliter scale, Rev. Mod. Phys. 77 (3) (2005) 977.
[53] T. Kotnik, G. Pucihar, D. Miklavčič, Induced transmembrane voltage and its correlation with electroporation-mediated molecular transport, J. Membr. Biol. 236 (1) (2010) 3–13.
[54] S. Carson, J. Wilson, A. Aksimentiev, M. Wanunu, Smooth DNA transport through a narrowed pore geometry, Biophys. J. 107 (10) (2014) 2381–2393.
[55] E. Stellwagen, Y. Lu, N.C. Stellwagen, Unified description of electrophoresis and diffusion for DNA and other polyions, Biochemistry 42 (40) (2003) 11745–11750.
[56] G.C. Wong, L. Pollack, Electrostatics of strongly charged biological polymers: ion-mediated interactions and self-organization in nucleic acids and proteins, Annu. Rev. Phys. Chem. 61 (2010) 171–189.
[57] A. Cherstvy, Electrostatic interactions in biological DNA-related systems, Phys. Chem. Chem. Phys. 13 (21) (2011) 9942–9968.
[58] X. Qiu, K. Andresen, J.S. Lamb, L.W. Kwok, L. Pollack, Abrupt transition from a free, repulsive to a condensed, attractive DNA phase, induced by multivalent polyamine cations, Phys. Rev. Lett. 101 (22) (2008) 228101.
[59] I. Koltover, K. Wagner, C.R. Safinya, DNA condensation in two dimensions, Proc. Natl Acad. Sci. 97 (26) (2000) 14046–14051.
[60] C. Herold, P. Schwille, E.P. Petrov, DNA condensation at freestanding cationic lipid bilayers, Phys. Rev. Lett. 104 (14) (2010) 148102.
[61] A.G. Cherstvy, E.P. Petrov, Modeling DNA condensation on freestanding cationic lipid membranes, Phys. Chem. Chem. Phys. 16 (5) (2014) 2020–2037.